Supporting Information

In situ QXAFS study on CO and H_2 adsorption on Pt in $[PtAu_8(PPh_3)_8]$-$H[PMo_{12}O_{40}]$ solid

Tomoki Matsuyama,[a] Taishi Suzuki,[a] Yuto Oba,[a] Soichi Kikkawa,[a] Sayaka, Uchida,[b] Junya Ohyama,[c] Kotaro Higashi,[d] Takuma Kaneko,[d] Kazuo Kato,[d] Kiyofumi Nitta,[d] Tomoya Uruga,[d] Keisuke Hatada,[e] Kazuki Yoshikawa,[e] Amelie Heilmaier,[e,f] Kosuke Suzuki,[g] Kentaro Yonesato,[g] Kazuya Yamaguchi,[g] Naoki Nakatani,[a] Hideyuki Kawasoko,[a,h] and Seiji Yamazoe*[a]

[a] Department of Chemistry, Graduate School of Science, Tokyo Metropolitan University, 1-1 Minami-osawa, Hachioji-shi, Tokyo 192-0397, Japan

[b] Department of Basic Science, School of Arts and Sciences, The University of Tokyo, 3-8-1 Komaba, Meguro-ku, Tokyo 153‐8902, Japan

[c] Faculty of Advanced Science and Technology, Kumamoto University, 2-39-1 Kurokami, Chuo-ku, Kumamoto-shi, Kumamoto 860-8555, Japan

[d] Center for Synchrotron Radiation Research, Japan Synchrotron Radiation Research Institute (JASRI), 1-1-1, Kouto, Sayo-cho, Sayo-gun, Hyogo 679-5198, Japan

[e] Department of Physics, University of Toyama, 3190 Gofuku, Toyama 930-8555, Japan

[f] Department of Chemistry, Ludwig-Maximilians-Universität (LMU), Butenandtstr. 5-13, 81377 Munich, Germany

[g] Department of Applied Chemistry, School of Engineering, The University of Tokyo, 7-3-1 Hongo, Bunkyo-ku, Tokyo 113-8656, Japan

[h] Precursory Research for Embryonic Science and Technology (PRESTO), Japan Science and Technology Agency (JST), 7, Gobancho, Chiyoda-ku, Tokyo 102-0076, Japan

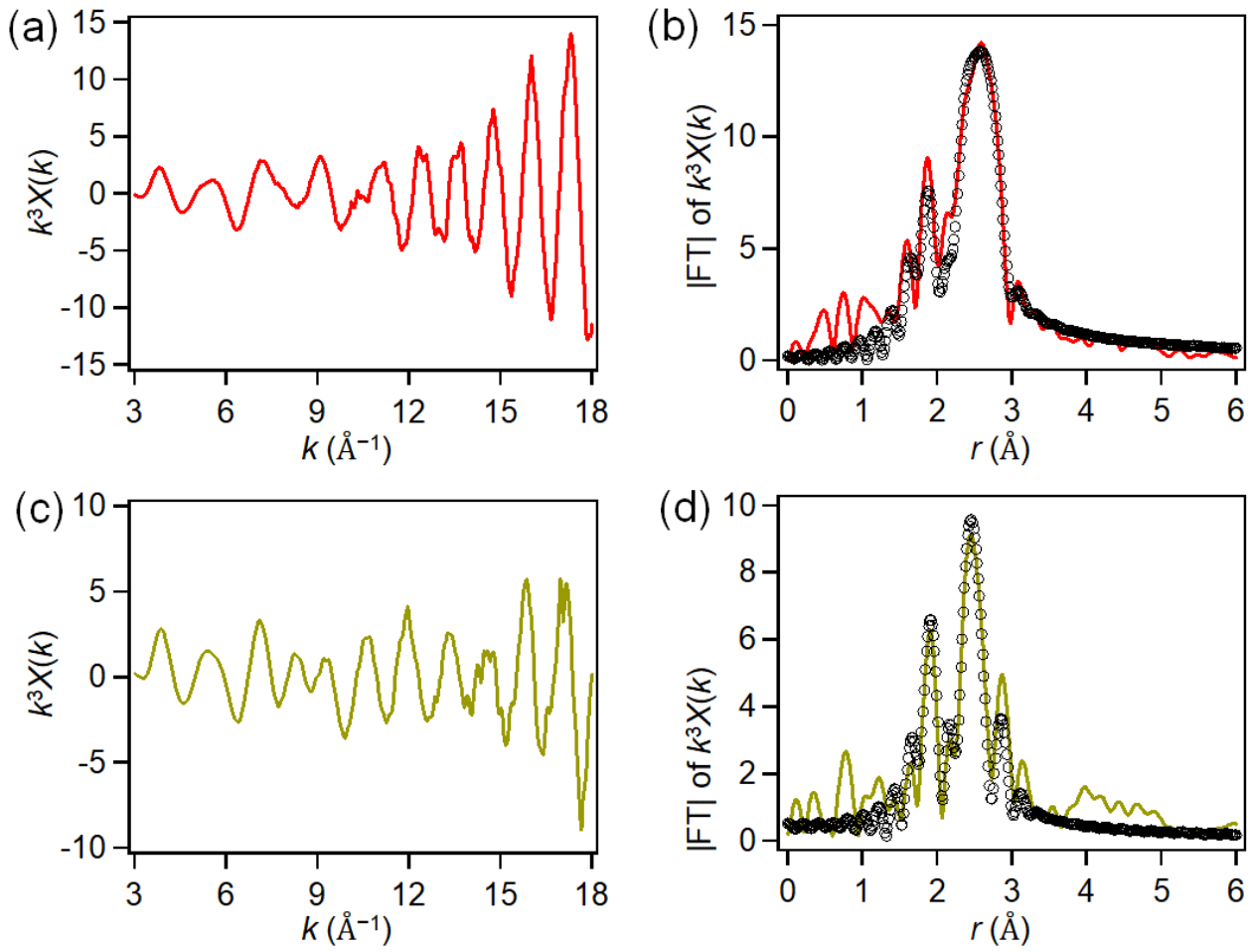

Fig. S1. Au L_3-edge (a) EXAFS oscillation and (b) FT-EXAFS spectra of **PtAu8-PMo12**, and (c) EXAFS oscillation and (d) FT-EXAFS spectra of **Au9-PMo12** measured at 10 K. The circles in (b) and (d) represent the fitting curves, whose parameters and results are listed in Table S1.

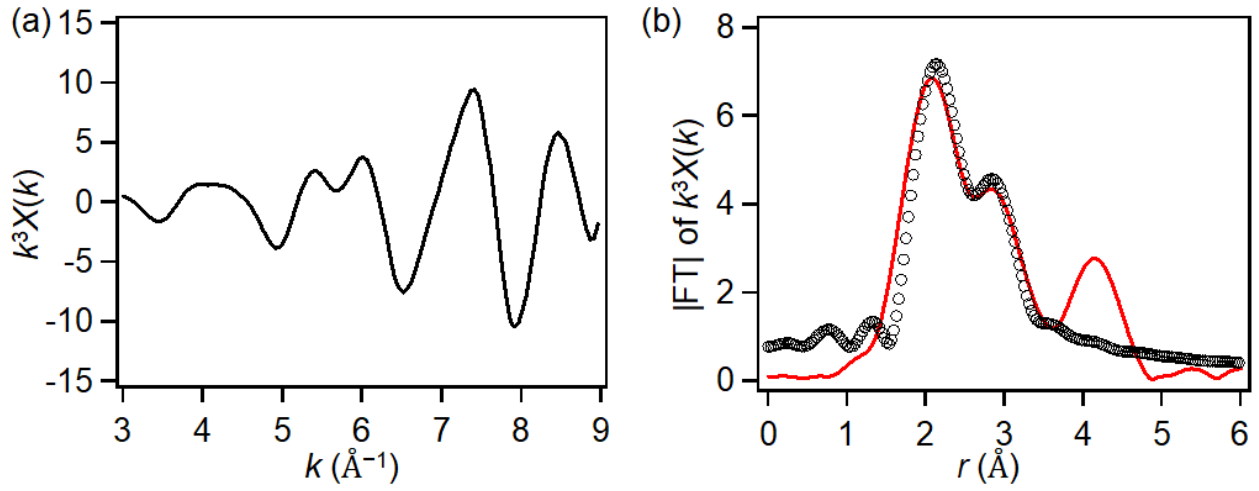

Fig. S2. Pt L_3-edge (a) EXAFS oscillation and (b) FT-EXAFS spectra of **PtAu8-PMo12** measured at 10 K. The circles in (b) represent the fitting curve, whose parameters and results are listed in Table S2.

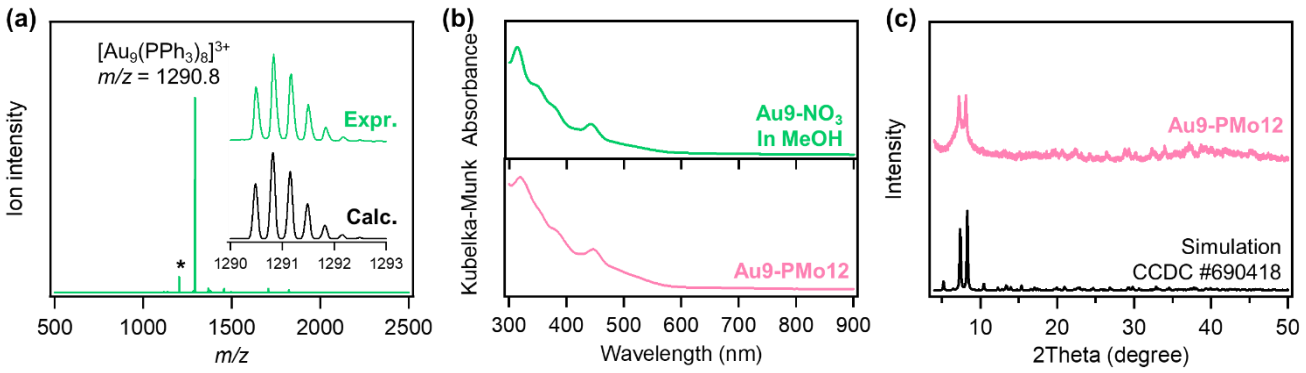

Fig. S3. Characterizations of **Au9-NO3** and **Au9-PMo12**. (a) Positive-ion mode ESI-MS of **Au9-NO3** in acetonitrile solution. Asterisk peak is the ligand-dissociated product in the analysis: $[Au_9(PPh_3)_7]^{3+}$. (b) UV-vis spectrum of **Au9-NO3** in methanol solution and DR-UV-Vis spectrum of **Au9-PMo12**. (c) Powder-XRD pattern of **Au9- PMo12**.

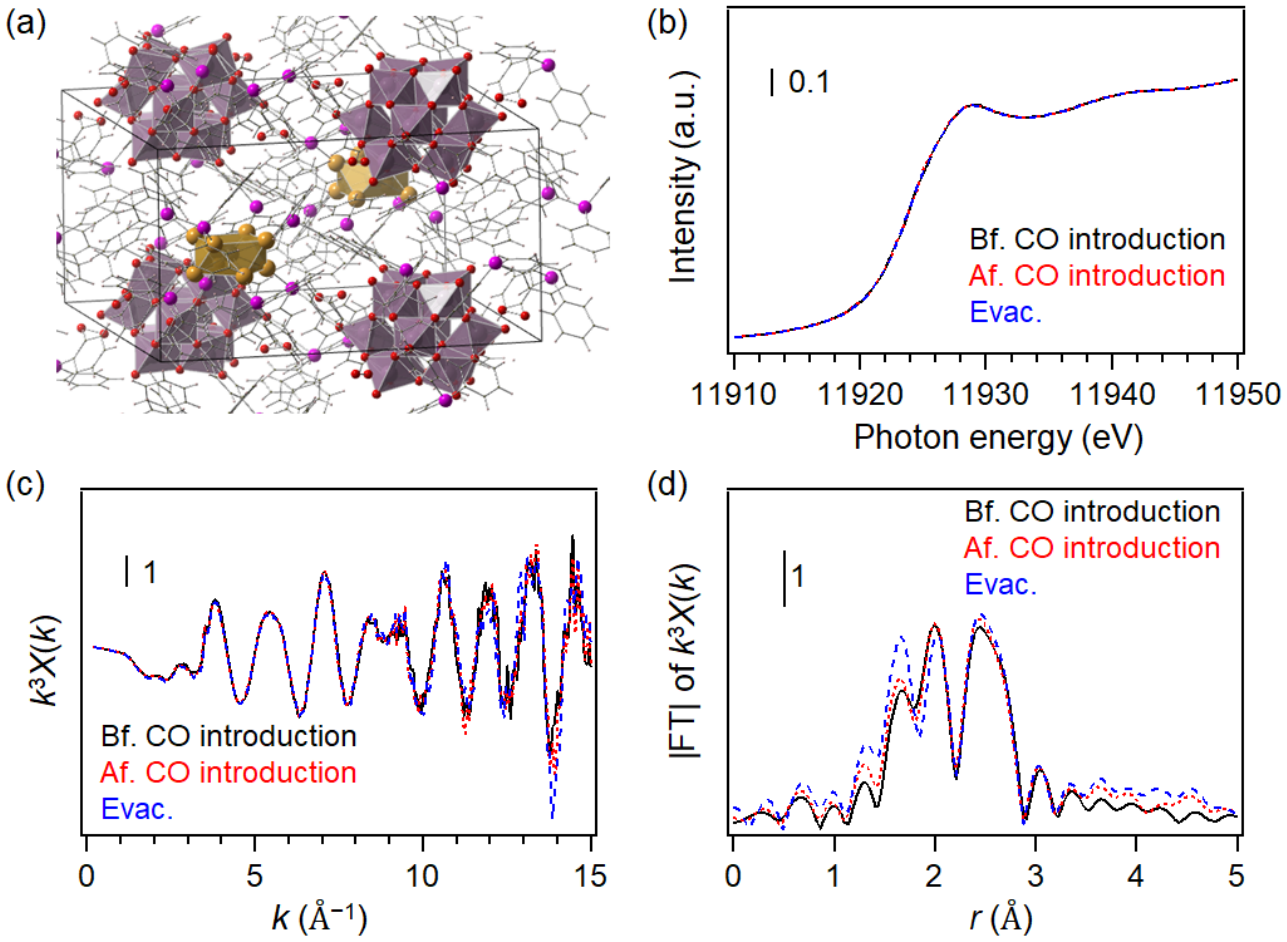

Fig. S4. (a) Crystal structure of **Au9-PMo12**.[1] Au L_3-edge (b) XANES, (c) EXAFS oscillations, and (d) FT-EXAFS spectra of **Au9-PMo12** before CO introduction (black), after CO introduction (red), and then after evacuation (blue).

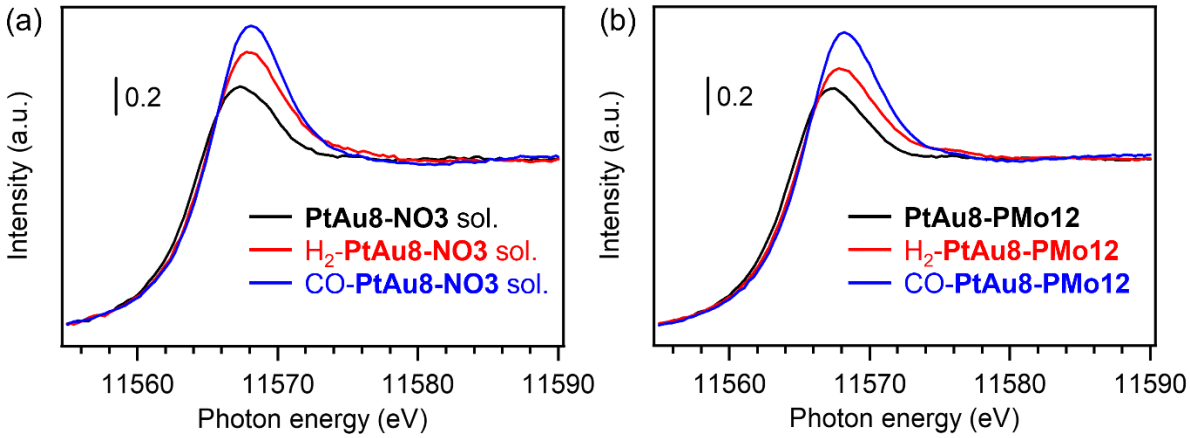

Fig. S5. Pt L_3-edge *in situ* XANES spectra of (a) **PtAu8-NO3** in acetonitrile and (b) **PtAu8-PMo12** in the solid state. The XAFS data were measured in BL01B1 at SPring-8 facility with using Si(111) mirror to monochromize the incident X-ray.

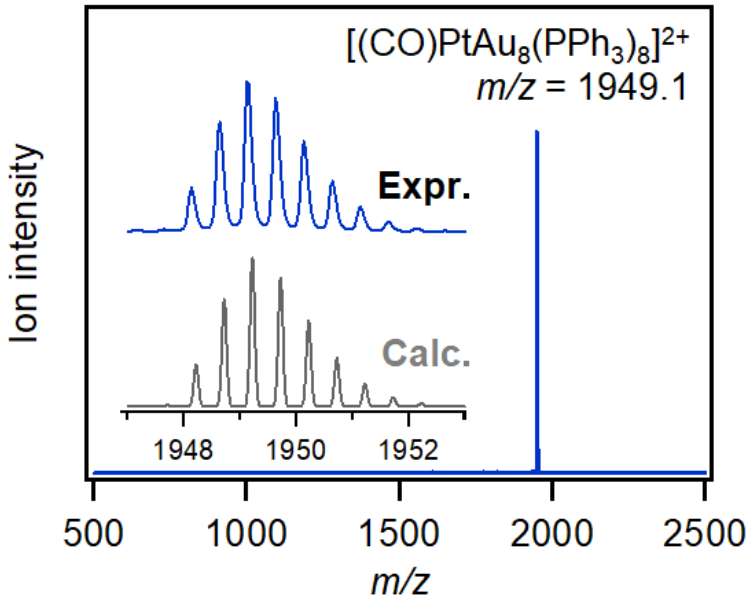

Fig. S6. Positive-ion mode ESI-MS of CO-**PtAu8-PMo12** dissolved in acetonitrile.

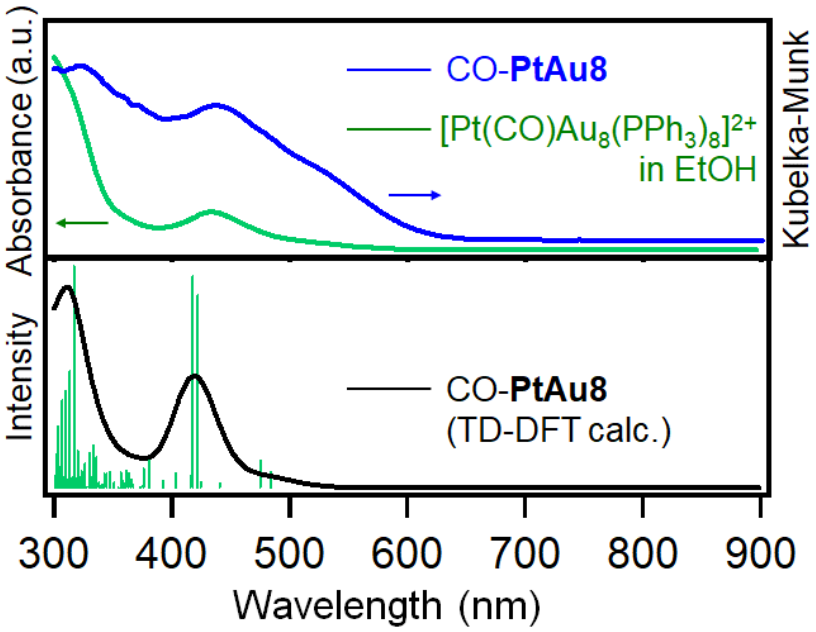

Fig. S7. UV-vis spectrum of CO adsorbed **PtAu8** ($[Pt(CO)Au_8(PPh_3)_8]^{2+}$) in ethanol, DR-UV-Vis spectrum of CO-**PtAu8-PMo12**, and calculated UV-Vis spectrum using the optimized structure of CO-**PtAu8** in Fig. 3c,

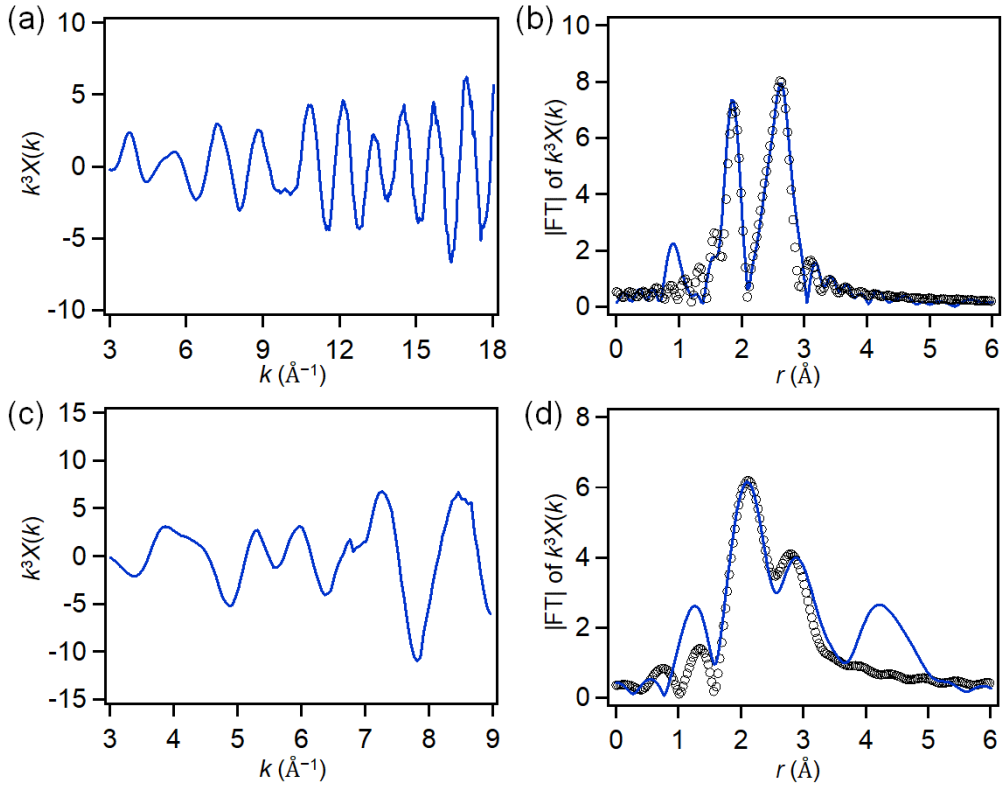

Fig. S8. Au L_3-edge (a) EXAFS oscillation and (b) FT-EXAFS, and Pt L_3-edge (c) EXAFS oscillation and (d) FT-EXAFS of CO-**PtAu8-PMo12** measured at 10 K. The circles in (b) and (d) represent the fitting curves, whose parameters and results are listed in Table S1.

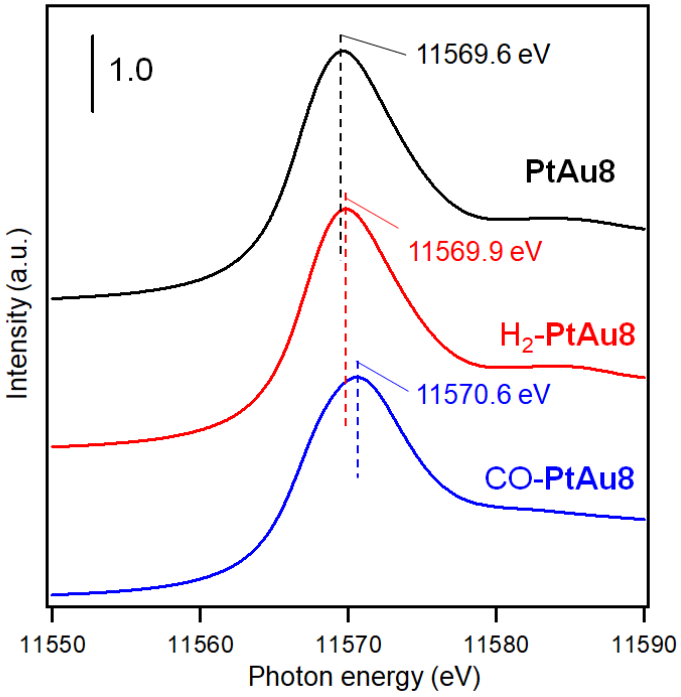

Fig. S9. Simulated Pt L_3-edge XANES of the crown-motif **PtAu8**, H_2-**PtAu8** (using optimized structure in Fig 3f), and the chalice-motif CO-**PtAu8** (using optimized structure in Fig. 3c. Energy calibration was carried out using the peak energy (11569.6 eV) of **PtAu8-PMo12** in Fig. 3a.

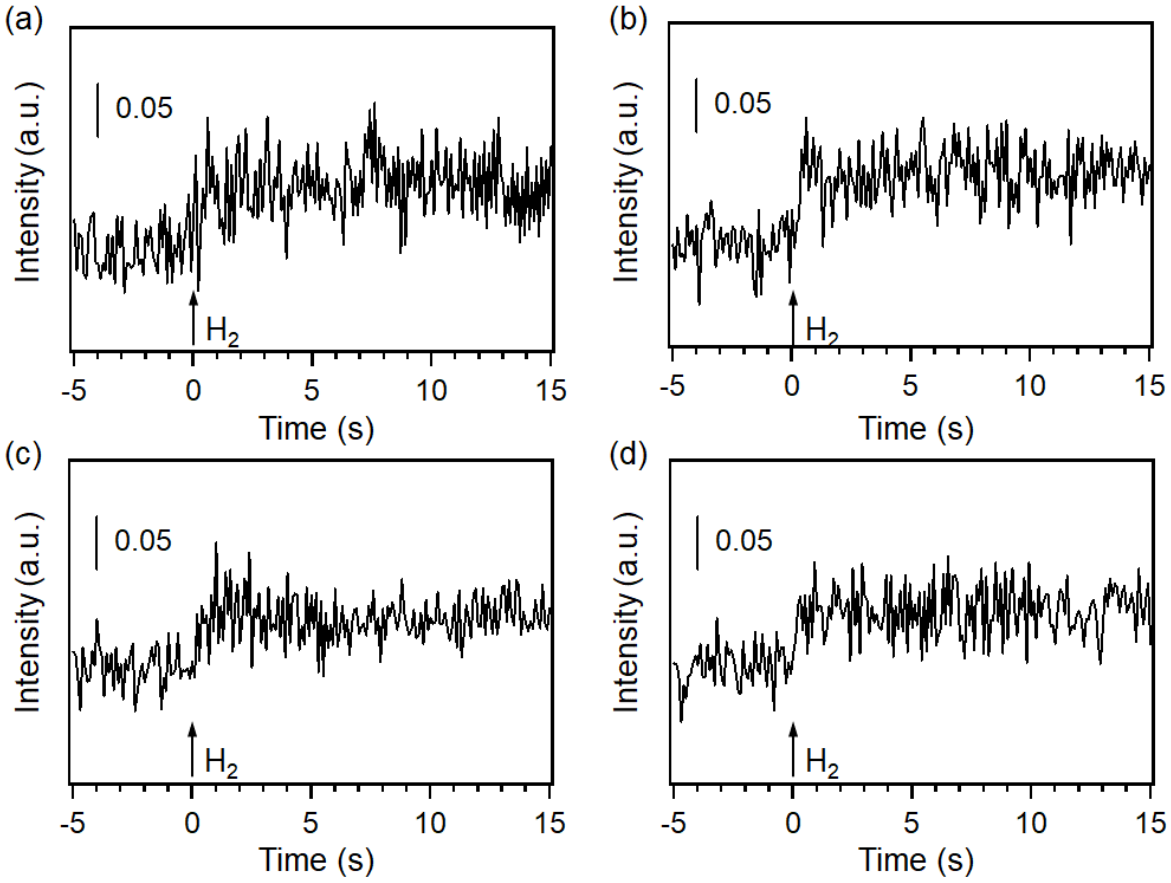

Fig. S10. Time course of peak intensity at 11570 eV in Pt L_3-edge XANES of **PtAu8-PMo12** during H_2 introduction: (a) 1st H_2 introduction, (b) 2nd H_2 introduction after evacuation of (a), (c) 3rd H_2 introduction after evacuation of (b), (d) 4th H_2 introduction after evacuation of (c).

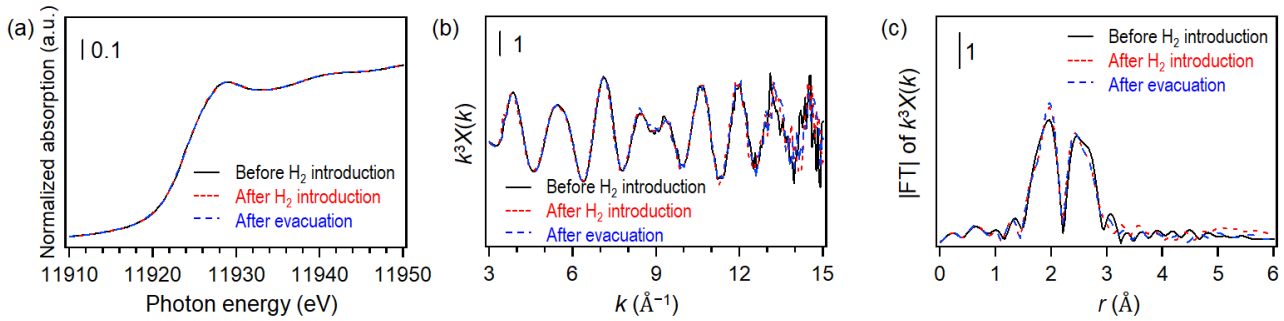

Fig. S11. Au L_3-edge (a) XANES, (b) EXAFS oscillations and (c) FT-EXAFS spectra of **Au9-PMo12** before and after H_2 introduction and after evacuation.

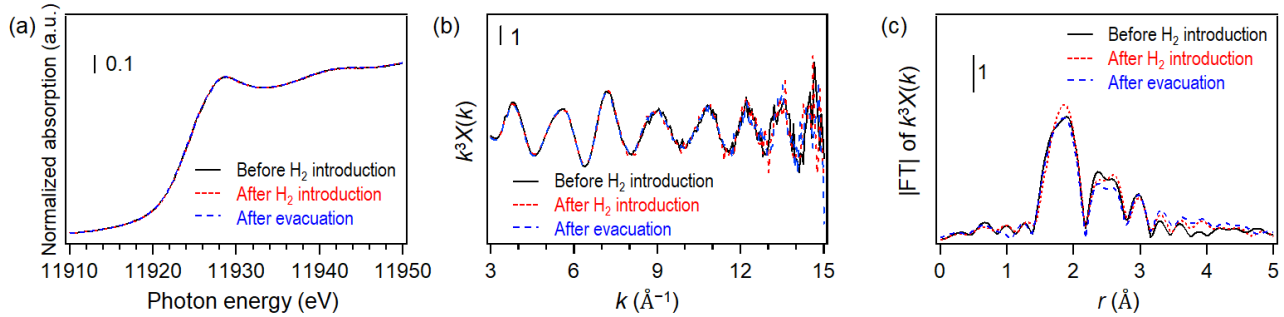

Fig. S12. Au L_3-edge (a) XANES, (b) EXAFS oscillations and (c) FT-EXAFS spectra of **PtAu8-PMo12** before and after H_2 introduction and after evacuation.

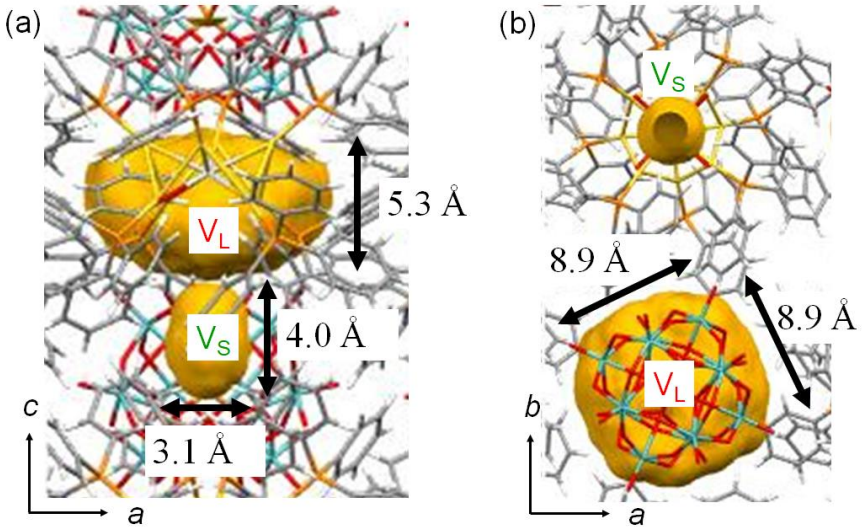

Fig. S13. Size of the closed voids in **PtAu8-PMo12**.

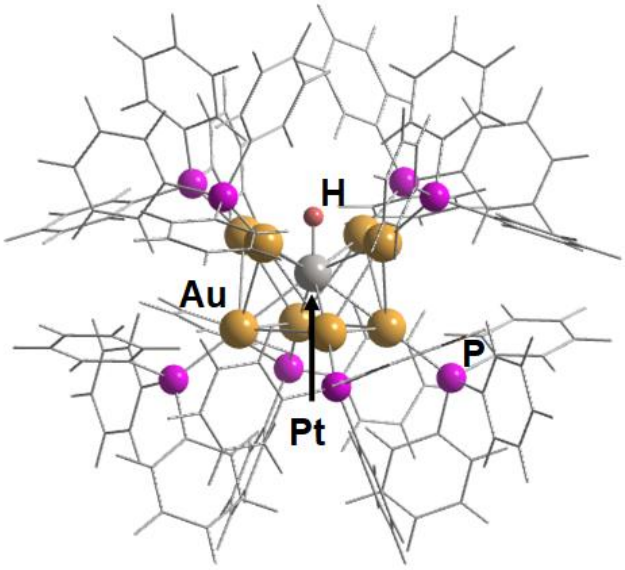

Fig. S14. Optimized structure of H-**PtAu8**.

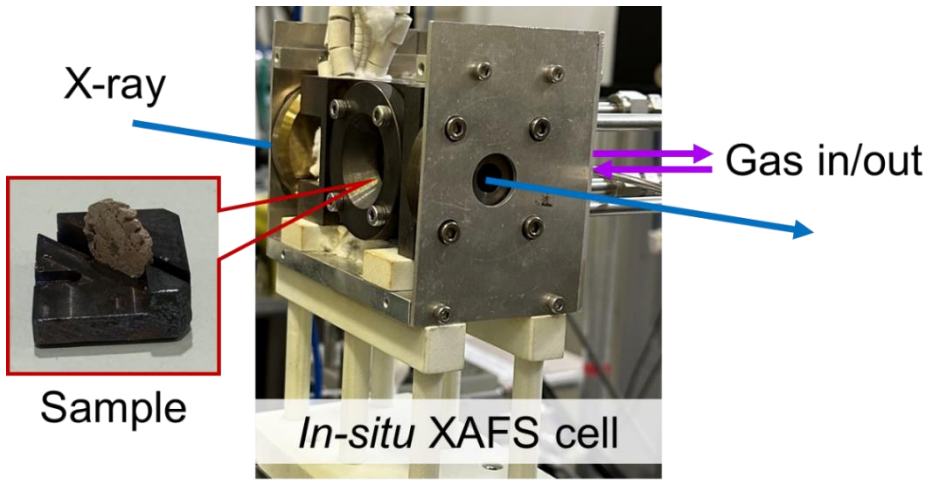

Fig. S15. Experimental setup for *in situ* XAFS measurement of solid samples at SPring-8.

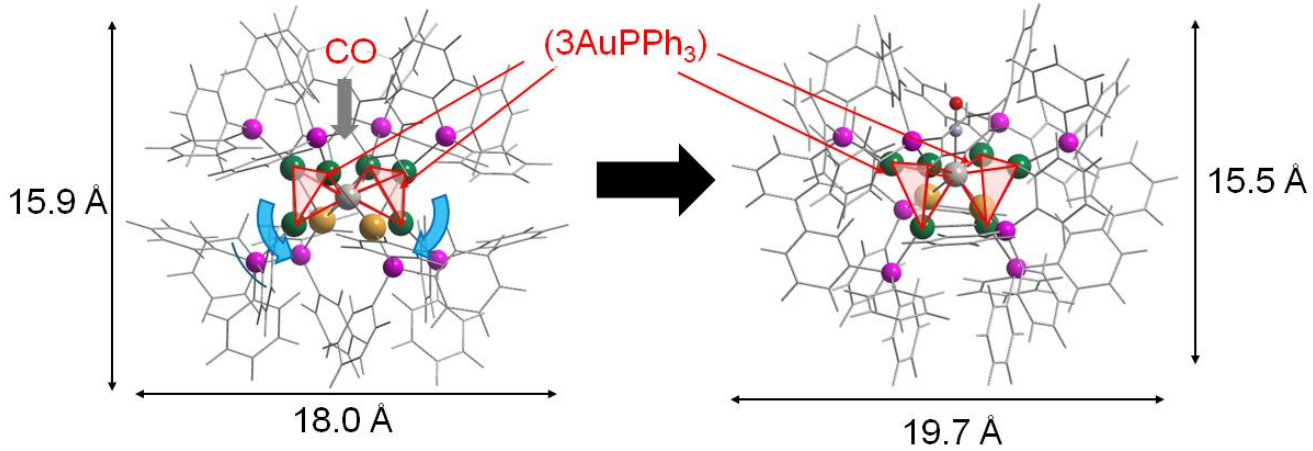

Scheme S1. Proposed structural isomerization mechanism from crown-motif **PtAu8** to chalice-motif **PtAu8** and cluster size obtained by optimized structures of crown-motif **PtAu8** and chalice-motif **PtAu8** by DFT calculations. Color; gray: Pt, green: Au in ($3AuPPh_3$) unit, pink: P.

Table S1. Curve fitting results of Au L_3-edge FT-EXAFS spectra for **PtAu8-PMo12**, CO-**PtAu8-PMo12**, and **Au9-PMo12**.

Samples	Bonds	CNs	*r* (Å)	σ^2	R-factor(%)
PtAu8-PMo12	Au-P	1.4 (2)	2.20 (3)	0.003 (2)	13.2
	Au-Pt	1.4 (1)	2.66 (2)	0.002 (1)	
	Au-Au	2.3 (2)	2.80 (2)	0.004 (2)	
CO-**PtAu8-PMo12**	Au-P	1.0 (2)	2.23 (3)	0.002 (1)	14.9
	Au-Pt	1.3 (1)	2.69 (2)	0.003 (1)	
	Au-Au	3.6 (7)	2.93 (11)	0.014 (11)	
Au9-PMo12	Au-P	1.4 (2)	2.28 (4)	0.004 (3)	11.4
	Au-Au1	1.4 (1)	2.67 (2)	0.003 (2)	
	Au-Au2	1.9 (2)	2.78 (3)	0.005 (2)	

CNs: coordination numbers, *r*: bond distance, σ^2: Debye–Waller factor.

Numbers in parentheses represent uncertainties. The reliability factor (R-factor) is defined as: R-factor $= \{\Sigma[k^3 \chi_{obs}(k) - k^3 \chi_{cal}(k)]^2 / \Sigma[k^3 \chi_{obs}(k)]^2\}^{1/2}$ where, χ_{obs} and χ_{cal} correspond to the observed and calculated data, respectively.

Table S2. Curve fitting results of Pt L_3-edge FT-EXAFS spectra for **PtAu8-PMo12** and CO-**PtAu8-PMo12**.

Samples	Bonds	CNs	*r* (Å)	σ^2	R-factor(%)
PtAu8-PMo12	Pt-Au	7.8 (3)	2.63 (3)	0.003 (2)	12.3
CO-**PtAu8-PMo12**	Pt-C	1.3 (3)	1.81 (10)	0.020 (17)	12.0
	Pt-Au	8.0 (4)	2.64 (3)	0.005 (4)	

CNs: coordination numbers, *r*: bond distance, σ^2: Debye–Waller factor.

Numbers in parenthesezs represent uncertainties. The reliability factor (R-factor) is defined as: R-factor $= \{\Sigma[k^3 \chi_{obs}(k) - k^3 \chi_{cal}(k)]^2 / \Sigma[k^3 \chi_{obs}(k)]^2\}^{1/2}$ where, χ_{obs} and χ_{cal} correspond to the observed and calculated data, respectively.

Table S3. Structural parameters of CO-**PtAu8** in Au L_3- and Pt L_3-edges obtained by the DFT calculation.

Sample	Edge	Bonds	CNs	*r* (Å)
$[Pt(CO)Au_8(PPh_3)_8]^{2+}$	Au L_3	Au-P	1.0	2.43[2.30]
		Au-Pt	1.0	2.79[2.64]
		Au-Au	3.8	3.14[2.97]
	Pt L_3	Pt-C	1.0	1.91[1.81]
		Pt-Au	8.0	2.79[2.64]

Bond lengths determined by the average bond lengths for the model structures. Numbers in square brackets are bond lengths reduced to 94.6% of their original values.[2]

References

1 M. Schulz-Dobrick and M. Jansen, *Z. Anorg. Allg. Chem.*, 2008, **634**, 2880–2884.

2 Y. Fujiki, T. Matsuyama, S. Kikkawa, J. Hirayama, H. Takaya, N. Nakatani, N. Yasuda, K. Nitta, Y. Negishi and S. Yamazoe, *Commun. Chem.*, 2023, **6**, 129.